Effect of Pressure Rate on Rate and State Frictional Slip

J. W. Rudnicki[1], Y. Zhan[2]

[1]Department of Civil and Environmental Engineering and Department of Mechanical Engineering, Northwestern University, Evanston, IL 60208-3109
[2]School of Civil and Resource Engineering, University of Science and Technology Beijing, No. 30, Xueyuan Road, Haidian District, Beijing, 100083, P. R. China

Key Points:

- Slip instabilities occur during the duration of a representative experiment in a limited range of pressure rate and diffusivity
- Identifies a pressure rate above which slip events are strongly damped by a rapid decrease of effective stress
- Interaction between fluid diffusion and pressure rate affects the type, frequency, and magnitude of slip events

Corresponding author: J. W. Rudnicki, `jwrudn@northwestern.edu`

Abstract

This paper analyzes the effects of pore pressure rate for a spring - block system that is a simple model of a laboratory experiment. Pore pressure is increased at a constant rate in a remote reservoir and slip is governed by rate and state friction. The frequency of rapid slip events increases with the increase of a nondimensional pressure rate that is the ratio of the time scale of frictional sliding to that for pressure increase. As the pressure rate increases, the more rapid increase of pore pressure on the slip surface quickly stabilizes slip events due to rate and state friction. Rate and state and pressure rate effects interact in a limited range of pressure rate and diffusivity. This range includes pressure rates and diffusivities representative of recent laboratory experiments.

Plain Language Summary

Recent field observations have identified fluid injection as an important factor in causing the dramatic increase of earthquakes in the central US and recent laboratory experiments have observed effects of fluid pressure rate on frictional sliding. This paper studies a simple model of a laboratory experiment: a block resting on a frictional surface and pulled by a spring. The frictional resistance to sliding depends on the rate and history of sliding. Fluid pressure is increased at a constant rate at a distance remote from the surface. The paper calculates the types and characteristics of rapid slip events and their dependence on the pressure rate and how fast fluid can diffuse from the reservoir to the frictional surface.

1 Introduction

Recent attention on the effects of pore fluid on failure has been stimulated by the dramatic increase of earthquakes in the mid-continental US (Ellsworth, 2013). Most of these events appear to be associated with the injection of waste water from hydraulic fracturing (Horton, 2012; Keranen et al., 2013, 2014; Weingarten et al., 2015; Barbour et al., 2017; Goebel et al., 2017) There is not yet any clear understanding of why these earthquakes occur and whether induced slip will be seismic or aseismic. The nearness of stress on faults to a critical value, the orientation and location of faults relative to injection sites, and availability of permeability channels are certainly factors. Operational factors that affect the incidence of seismicity include the volume of fluids injected or withdrawn and the injection rate (Ellsworth, 2013).

Two indications of the importance of the pressure rate come from a field study and a numerical simulation. Weingarten et al. (2015) examined about 20,000 wells in the mid-continent US associated with seismicity and found that among various operational parameters, the injection rate had the best correlation with induced seismicity. Almakari et al. (2019) examined the effect of pore pressure rate on seismicity. They simulated the seismicity rate increase due to a ramp increase in pore pressure on a heterogeneous fault. They find that the seismicity rate increases with both pore pressure and rate, but that the effect of the rate is greater.

Although field observations are the ultimate test of the effects of pore fluid on failure, their interpretation is often complicated by uncertainty about the boundary conditions, state of stress, heterogeneity of hydrologic and mechanical structure, and history. Laboratory experiments, despite their limited size and time scales, offer a more controlled environment that can contribute insight into fundamental processes.

The motivation for this study is recent laboratory studies addressing the role of pressure rate in causing slip (French et al., 2016; Scuderi et al., 2017; Passelégue et al., 2018; Cappa et al., 2019; Noël et al., 2019; Wang et al., 2020). Three of these studies (French

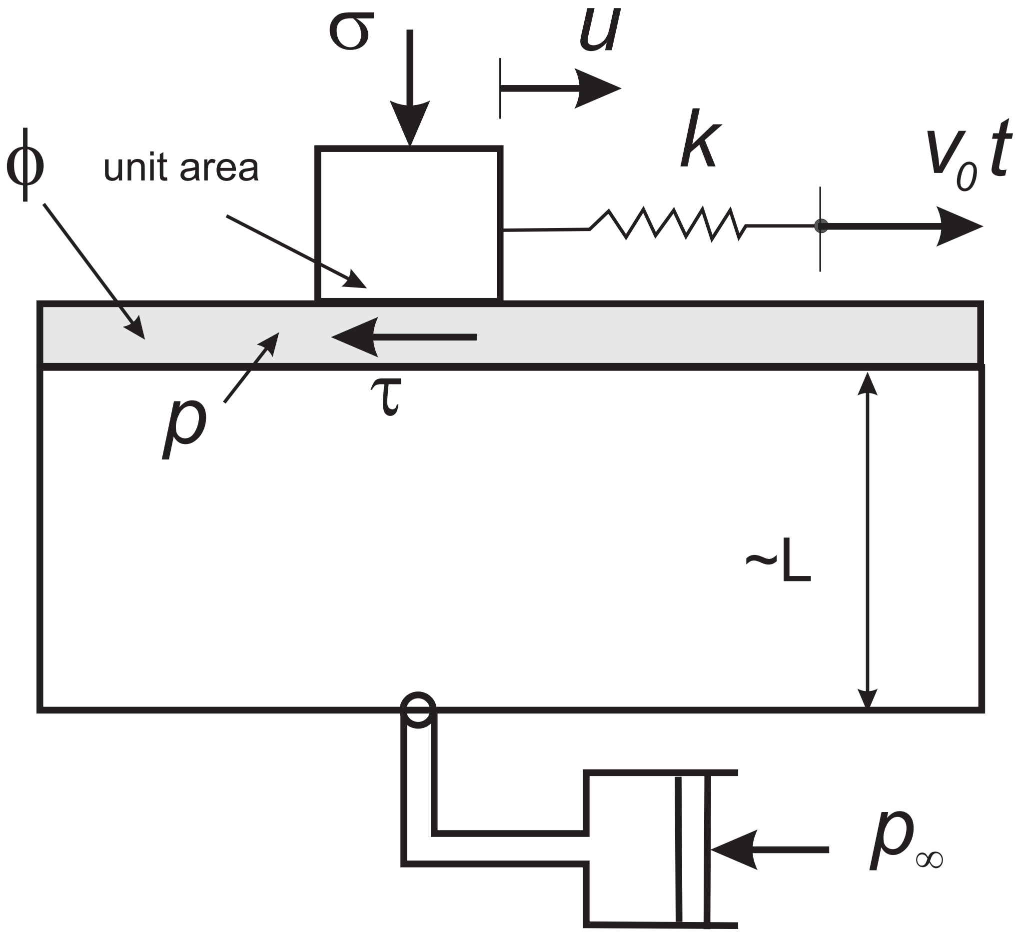

Figure 1. The spring - block model of Segall and Rice (1995)

et al., 2016; Passelégue et al., 2018; Wang et al., 2020) indicate that the pressure rate is more important than the pore pressure itself in failure.

This paper extends the spring - block model of Segall and Rice (1995) (Figure 1) to examine the effect of pressure rate. This system is an oversimplified model of crustal faulting, but it is a reasonable idealization of laboratory experiments in which slip occurs nearly simultaneously on the frictional surface. Segall and Rice (1995) showed that this system exhibits a wide spectrum of behavior that is further enriched by including the pressure rate. Despite the limitations of the model for crustal faulting, among their results are a constraint on the maximum pore pressure at depth that is consistent with the absence of an observed heat flow anomaly and the occurrence of aftershock-like instabilities.

In Segall and Rice (1995) sliding of the block on a porous layer is governed by rate and state (hereafter abbreviated RS) friction. In the last 50 years, an enormous amount of experimental work (Marone, 1998) has documented that a RS formulation is an accurate description of rock friction. In this formulation, friction depends on the sliding velocity and a variable that characterizes the state of the surface. Simulations using RS friction describe many observed features of earthquakes.

The goal of this study is to examine the effect of imposed pore pressure rate on RS frictional slip in a simple situation that avoids complicating effects. In particular, we examine the case of constant pore pressure rate with imposed displacement. We focus on the effects of the interaction of the time scales of fluid diffusion, pore pressure rate, and RS frictional slip on type, magnitude and frequency of slip events. The results can aid in the interpretation of laboratory tests and, to a lesser extent, field studies.

2 Formulation

The model is that of Segall and Rice (1995) shown in Figure 1. A block of unit area subjected to a constant normal stress σ slides on a thin porous layer. The block is connected to a spring with stiffness k. Slip of the block is u. The other end of the spring is displaced at a constant rate v_0. Thus, the shear stress due to motion of the block is

$$\tau = k\left(v_0 t - u\right) \tag{1}$$

The layer has porosity ϕ and a pore pressure p. There is a flux of fluid to the layer from a remote reservoir with a pore pressure p_∞. The remote reservoir is at some nominal distance L from the layer. Consistent with the discrete spring-mass system, Segall and Rice (1995) adopt the approximation of Rudnicki and Chen (1988) that the fluid mass flux into the layer is proportional to the difference between the remote pore pressure p_∞ and the pore pressure in the layer. Consequently the equation expressing conservation of fluid mass is

$$c^*\left(p_\infty - p\right) = \dot{p} + \dot{\phi}/\beta \tag{2}$$

where ϕ is now the inelastic part of the porosity, the superposed dot denotes the time derivative and c^* is the reciprocal of a time constant for fluid diffusion. c^* can be expressed in terms of a diffusivity c as $c^* = c/L^2$. $\beta = \phi_0\left(\beta_f + \beta_\phi\right)$ is a compressibility where β_f is the compressibility of the pore fluid, β_ϕ is the compressibility of the pore space and ϕ_0 is the initial porosity. In an extension of Segall and Rice (1995) we take the far-field pore pressure to increase linearly with time:

$$p_\infty = p_\infty^0 + \dot{p}_\infty t \tag{3}$$

Slip on the layer is described by RS friction (Dieterich, 1979; Ruina, 1983) of the form

$$\tau = (\sigma - p)\left[\mu_0 + a\ln\left(v/v_0\right) + b\left(\theta/\theta_0\right)\right] \tag{4}$$

where μ_0 is the nominal friction coefficient, $v = du/dt$ is the slider velocity, and θ is a state variable. Reference values of the velocity and state are v_0 and θ_0 and a and b are constitutive parameters. Two versions of the equation for the evolution of state are typically used: the "slip" law and the "aging" or "slowness" law. Bhattacharya et al. (2015) have shown that the slip law fits experimental data better, particularly at larger velocity steps. Consequently, we use the slip law:

$$\dot{\theta} = -\left(v\theta/d_c\right)\ln\left(v\theta/d_c\right) \tag{5}$$

where d_c is a characteristic sliding distance.

For $b - a > 0$ the response is velocity weakening. For $b - a < 0$ the response is velocity strengthening. Ruina (1983) showed that for velocity weakening the response can be unstable, in the sense that small perturbations grow exponentially in time, when the spring stiffness is less than a critical value k_{crit}. For drained response (constant pore pressure corresponding to rapid fluid diffusion),

$$k_{crit} = (\sigma - p)(b - a)/d_c \tag{6}$$

Note that an increase in pore pressure reduces k_{crit} and, thus, stabilizes response.

Segall and Rice (1995) proposed the following evolution equation for the porosity:

$$\dot{\phi} = -\left(\phi - \phi_{ss}\right) v/d_c \tag{7}$$

where the steady state value is given by $\phi_{ss} = \phi_0 + \varepsilon \ln\left(v/v_0\right)$. The initial value of the porosity is ϕ_0 and ε is a parameter that gives the magnitude of the effect. They show that this formulation describes well the data of Marone et al. (1990) on porosity changes with shear of simulated fault gouge and find that $\epsilon = 1.7 \times 10^{-4}$.

The final ingredient is the equation of motion:

$$\dot{\tau} = k\left(v_0 - v\right) - \eta\dot{v} \tag{8}$$

The second term on the right employs the radiation damping approximation to inertia, i.e. mdv/dt is replaced by ηv where $\eta = G/2v_s$. G is the shear modulus and v_s is the shear wave velocity (Rice & Tse, 1986; Rice, 1993).

Differentiating (4) and setting equal to (8) along with (2), (5), and (7) yield a system of four ordinary differential equations for V, p, θ, and ϕ. It is advantageous to rewrite these equations in the non-dimensional variables $V = v/v_0$, $T = v_0 t/d_c$, $\Sigma = \mu_0\left(1 - p/\sigma\right)$, $P = p/\sigma$, $\hat{\eta} = \eta v_0/\sigma$, $\hat{c} = c^* d_c/v_0$, $\hat{\beta} = \sigma\beta$, $\hat{\theta} = \theta v_0/d_c$, $\hat{\phi} = \phi - \phi_0$ and $\hat{k} = k/k_c$ where k_c is the critical stiffness (6) based on the initial value of the far-field pore pressure p_∞^0. With these non-dimensionalizations $\dot{P}_\infty = \dot{p}_\infty d_c/v_0\sigma$.

3 Parameter Values

Although the model is simple, there are a quite a few parameters. Some of these are uncertain and others vary widely. In the simulations, we will vary two non-dimensional parameters, $\dot{P}_\infty$ and $\hat{c}$. We choose values representative of the experiments of French et al. (2016) for Berea and Darley Dale sandstones. These are similar to those for the Fontainebleau sandstone used by Noël et al. (2019). In Table 1, French et al. (2016) give imposed slip rates ranging from 1.6×10^{-7} to 6.5×10^{-7} m/s. We take $v_0 = 3.0 \times 10^{-7}$ m/s as representative. Lateral confining stresses range from 42 to 62 MPa and we take $\sigma = 50$ MPa. The initial value of the pore pressure is about 10 MPa. This gives $P_\infty^0 = 0.2$. Using $v_s = 2.5 \times 10^3$ m/s (Green & Wang, 1994) and $G = 10^4$ MPa gives $\hat{\eta} \approx 10^{-8}$. Pore pressure rates vary from 0.3 to 1.0 MPa/min.

French et al. (2016) give 10^{-14} m^2 and 10^{-13} m^2 for the permeabilities of the two sandstones. The diffusivity is given by $c = k\gamma/\nu S$ where k is the permeability, γ is the weight density of water (9.81×10^4 Pa), ν is the dynamic viscosity of water (10^{-3} Pa s) and S is a storage coefficient, equal to 1.5×10^{-6} m^{-1} (Green & Wang, 1994). These values give $c = 0.065$ m^2/s for Berea. Dividing by the square of the specimen length (50.8 mm) gives $c^* = 25.2$ s^{-1}.

Although French et al. (2016) discuss their results in terms of RS friction, they do not measure the parameters in their experiment. From their experiments on simulated fault gouge, Marone et al. (1990) find $d_c = 0.02$ mm. For this value of d_c and v_0, the duration of the experiment (approximately 4000 s) corresponds to $T = 60$. For values used by Segall and Rice (1995) as representative of crustal faulting, $d_c = 0.01$ m and $v_0 = 0.03$ m/year, $T = 100$ corresponds to 33.3 years.

Segall and Rice (1995) infer $\epsilon = 1.7 \times 10^{-4}$ from the experiments of Marone et al. (1990) and $\beta = 1.4 \times 10^{-4}$MPa^{-1} from experiments of Zoback and Byerlee (1976). We use these. Using the larger of the pressure rates (1 MPa/min), $v_0 = 3.0 \times 10^{-7}$m/s, and $d_c = 0.02$ mm gives $\dot{P}_\infty = 0.022$.

In addition, we adopt the representative RS frictional parameters used by Segall and Rice (1995), $a = 0.010$ and $b = 0.015$, and take the nominal friction coefficient as $\mu_0 = 0.64$ (French et al., 2016). Because $a < b$, the behavior is velocity weakening and a critical value of the stiffness for drained deformation is given by (6) . In their experiments, French et al. (2016) induce instability (resulting in rapid slip events) by reducing the lateral confining stress leading to a reduction of normal stress on the slip surface. For simplicity and in order to focus on the role of the pressure rate, we keep the normal stress σ constant and choose a value for the stiffness much less than the critical value for drained deformation (6). In particular, we arbitrarily take $\hat{k} = 0.1$. (Results for $\hat{k} = 0.5$ are shown in the Supporting Information).

Segall and Rice (1995) derive an expression for the critical stiffness as a function of the non-dimensional diffusivity $\hat{c}$. The ratio of the critical stiffness to that for drained deformation (6) is

$$K(\hat{c}) = 1 - \frac{\epsilon\mu_0}{\beta(\sigma - p)(b - a)} F(\hat{c}) \tag{9}$$

where $F(\hat{c}) \to 0$ as $\hat{c} \to \infty$, corresponding to very rapid diffusion and drained conditions (pore pressure equal to that in the reservoir), and $F(\hat{c}) \to 1$ as $\hat{c} \to 0$, corresponding to very slow diffusion and undrained conditions (no change in fluid mass).

For the values of parameters of the experiment, $c = 0.065$ m^2/s, $v_0 = 3.0 \times 10^{-7}$ m/s and $d_c = 0.02$ mm, $\hat{c} = 1.68 \times 10^3$ and from (9) $K \approx 1$, indicating that deformation is essentially drained. However, French et al. (2016) cite Zhang and Tullis (1998) in arguing that permeabilities could be as small as 10^{-17} m^2 for gouge layers formed by frictional shearing of surfaces and Wibberley and Shimamoto (2003) have found permeabilities as low as 10^{-19} m^2 in samples from the fault core of the Median Tectonic Line. These give values of $\hat{c}$ three to five orders of magnitude smaller.

4 Simulations

The simulations are started with a small perturbation from steady sliding: $v(0) = 1.05\ v_0$. Other initial conditions are as follows: $\tau(0) = \mu_0 \left(\sigma - p^0_\infty\right)$, $p = p^0_\infty$, $\hat{\phi} = 0$, and $\hat{\theta} = v_0/v(0)$. Results are shown for $\hat{k} = 0.1$, two values of $\dot{P}_\infty$, 10^{-3} and 10^{-4}, and two values of the diffusivity, $\hat{c}$: 1.0 (Figure 2) and 10 (Figure 3). Figure 4 shows results for $\dot{P}_\infty = 10^{-2}$ and two values of the diffusivity, $\hat{c} = 1.0$ and $\hat{c} = 10$.

If the first peak in Figure 2 is ignored (because it appears to be affected by the initial conditions), the maximum slip velocity for both pressure rates is about 30 ($e^{3.4}$) v_0 times the imposed velocity. For $\dot{P}_\infty = 10^{-3}$, the first event occurs at about $T \approx 50$ which is slightly before the end of the experiment of French et al. (2016), $T = 60$. Thereafter, the velocity peaks decay to $\approx 2.5\ v_0$ (slightly greater than v_0 because of the pressure rate). The initial period is $T \approx 37$ which decreases with time. The decay occurs because the increasing pressure reduces the effective stress (bottom panel) and, consequently, the value of k_{crit} (6), to zero at $T \approx 800$. For $\dot{P}_\infty = 10^{-4}$, the first event (again ignoring the initial peak) occurs at about 80. Thereafter, peaks of roughly similar magnitude occur with a period of about 93. The is no discernible decay in the magnitude of the peaks in slip but, because of the increasing pressure, the slip rate eventually decays to near v_0 but not until about at about $T \approx 8000$. The bottom panel shows the (non-dimensional) effective stress multiplied by μ_0. Because the total normal stress is constant, changes in stress reflect pore pressure changes of the opposite sign. Drops occur simultaneously with the slip events. For $\dot{P}_\infty = 10^{-3}$ the maximum stress drop is about 0.04 (a dimensional stress drop of $0.04 \times \sigma/\mu_0 = 3.1$ MPa). For $\dot{P}_\infty = 10^{-4}$ the stress drop is about the same. For values of $\dot{P}_\infty$ less than 10^{-4} the effect of the pore pressure change in the reservoir is minimal and the response is nearly entirely due to RS effects.

Figure 3 shows results for $\hat{c} = 10$. For $\dot{P}_\infty = 10^{-3}$ the maximum peak velocities ($e^{5.7} = 300$) is much greater than for $\hat{c} = 1$, the maximum stress drop is about the same (0.04) and the time between events is smaller (44). Again ignoring the first peak,

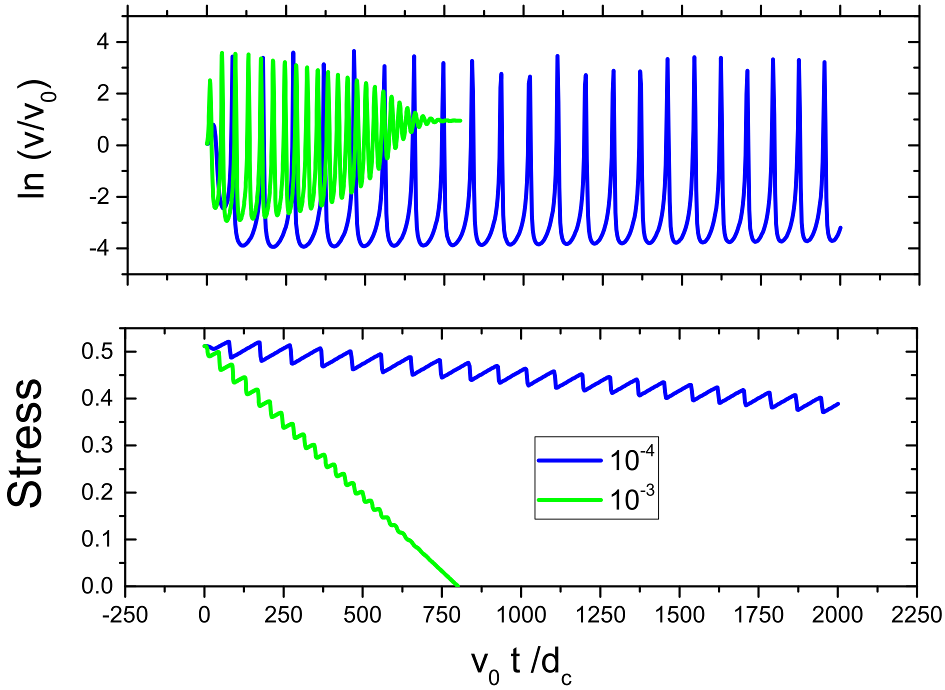

Figure 2. Upper panel shows logarithm of velocity (divided by v_0) and lower panel shows stress (divided by σ), $\Sigma = \mu_0 (1 - p/\sigma)$, for two values of $\hat{P}_\infty$: 10^{-4}, and 10^{-3} The abscissa is $T = v_0 t/d_c$ and $\hat{c} = 1$.

the first event occurs at $T \approx 50$. For $\dot{P}_\infty = 10^{-4}$, the magnitude of the peak velocities vary but with no obvious pattern. They do, however, eventually decay to near v_0 but, again, not until about $T \approx 8000$. The stress drops are slightly larger (0.46). If, again, the first slip event is ignored, the first peak occurs at $T = 108$.

According to (9), for $\hat{c} = 10$, the ratio of the critical stiffness to the critical stiffness for drained deformation (both based on the pore pressure p_∞^0) $K = 0.938$. Therefore, $\hat{c} = 10$ is close to drained conditions and there will be little difference in the response for larger values of $\hat{c}$. For $\hat{c} = 1$, $K = 0.51$, which is much closer to undrained response and, according to Figure 4 of Segall and Rice (1995), is in a range where $K(\hat{c})$ decreases rapidly with $\ln(\hat{c})$. For the parameters here undrained deformation is stable and the response is increasingly damped for smaller values of $\hat{c}$. Thus, the smaller peak velocities and stress drops in Figure 2, $\hat{c} = 1$, compared with Figure 3, $\hat{c} = 10$, reflect the stabilizing effects of dilatant hardening for conditions closer to undrained deformation.

For $\hat{c} = 0.1$, (see Supporting Information) $K = 0.09$, very close to undrained conditions. For $\dot{P}_\infty = 10^{-4}$, there are only a few small (maximum 1.3 v_0), slow (duration $\Delta T \approx 100$) slip events that decay quickly. For $\dot{P}_\infty = 10^{-3}$, there is one slow slip event with a peak velocity of about 3.7 v_0) which then decreases and levels off to a velocity of about 2.5 times the background rate. There are no discernible stress drops on the scale of the graph. For $\dot{P}_\infty = 10^{-3}$, there is still a significant downward trend to the stress that again reaches zero at $T = 800$. Responses for smaller values of $\hat{c}$ will be more strongly damped.

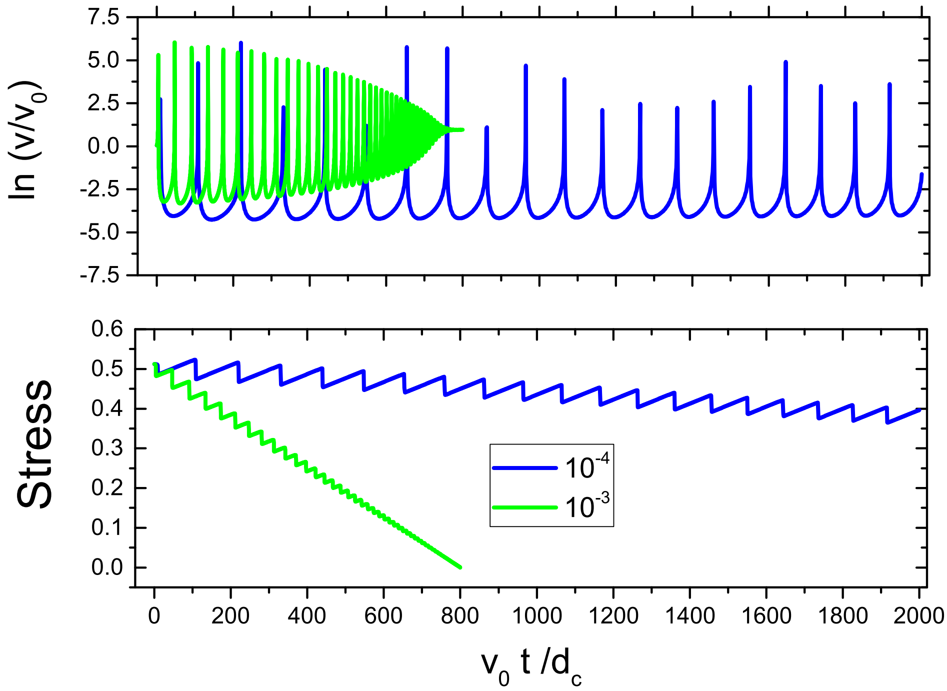

Figure 3. Same as Figure 2 for $\hat{c} = 10$.

Figure 4 shows the response for $\dot{P}_\infty = 10^{-2}$, representative of the laboratory value, for two values of $\hat{c}$: 1 and 10. The bottom panel shows that the frictional resistance decreases to zero at $T = 80$. For $\hat{c} = 10$, there are 12 slip events with slightly decreasing maximum slip rates before the end of the experiment ($T = 60$). The maximum slip rate is about 300 v_0, the maximum stress drop is about 3.1 MPa and the period is $\Delta T \approx 6$. For $\hat{c} = 1$, there is a single slow event followed by oscillations that are strongly damped because the response is closer to undrained deformation. For smaller diffusivities, the response is even more strongly damped.

5 Discussion

The simulations illustrate the effects of $\dot{P}_\infty$, the ratio of the characteristic time of the imposed rate of frictional slip to that of pressurization. For all the values of $\hat{c}$ and $\hat{k}$ considered, the frequency of events increases with $\dot{P}_\infty$. As the pore pressure in the reservoir increases, the effective stress decreases, reducing the value of k_{crit} (6) and stabilizing the response. Eventually, the effective stress goes to zero and the response is completely stabilized: the slip velocity returns to about the imposed rate. This limit is attained more quickly for larger $\dot{P}_\infty$. For $\dot{P}_\infty = 10^{-2}$, representative of the experiment of French et al. (2016) and similar to that of Wang et al. (2020) and the simulation of Almakari et al. (2019), it occurs about 30% beyond the end of the experiment. For $\dot{P}_\infty$ within the range of 10^{-4} to 10^{-3} the interaction of RS effects and the increase of pore pressure are most significant. For values smaller than this the pressure rate has little effect until very long times and the occurrence of slip events is dominated by RS effects.

The response also depends on $\hat{c}$, the ratio of the characteristic time of the imposed rate of frictional slip to that of fluid diffusion. The magnitude of the stress drop and peak velocities decrease with decreasing $\hat{c}$. The decrease is most dramatic for $\hat{c} = 0.1$, reflect-

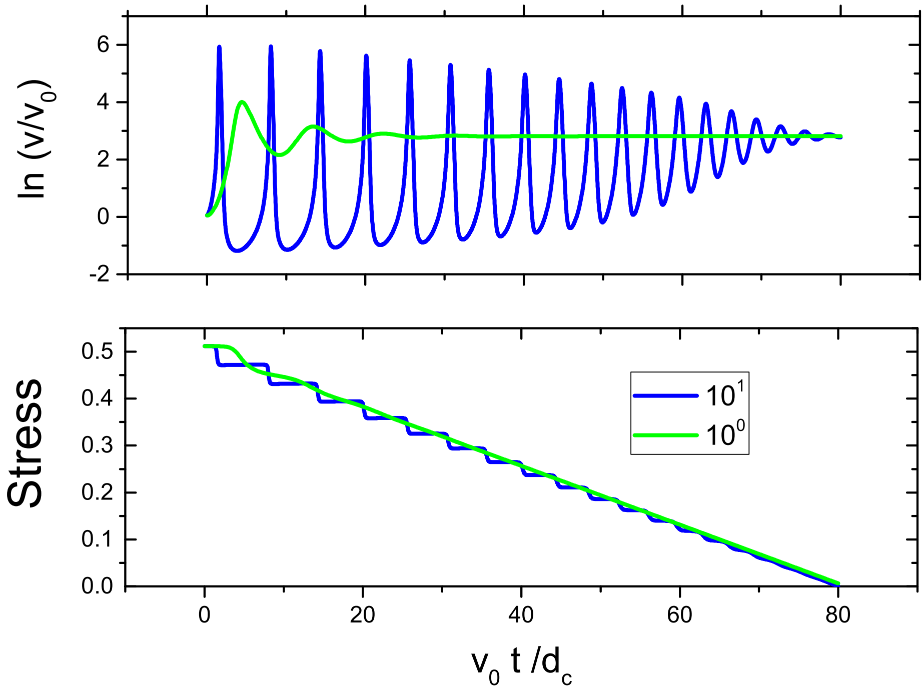

Figure 4. Same as Figure 2 for $\dot{P}_\infty = 10^{-2}$ and $\hat{c} = 1$ and 10.

ing the stabilizing effect of dilatant hardening as undrained conditions are approached. This stabilizing effect begins to dominate for $\hat{c}$ less than about 1. For $\hat{c}$ greater than about 10 conditions are effectively drained and largely independent of $\hat{c}$.

The analysis gives an indication of the possibility of slip instabilities in representative experiments. If we assume instabilities occur when the slip velocity is more than an order of magnitude greater than the background rate and must occur before the end of a representative experiment, $T = 60$, then they can occur only in a limited range of values of $\hat{k}$, $\hat{c}$ and $\dot{P}_\infty$. For $\hat{k} = 0.5$ (see Supporting Information) none occur because the peak slip velocities are too small. For $\hat{k} = 0.1$ none occur for $\hat{c} = 0.1$ because of the strong dilatant hardening when deformation is relatively undrained. For $\hat{c} = 10$ and $\hat{c} = 1$, instabilities occur only for $\dot{P}_\infty = 10^{-3}$ and 10^{-2}. These are in the range of the experiments of French et al. (2016), at least if the lower values of the permeability that they cite are appropriate.

Two other experiments that increase pressure in stepwise fashion at rates similar to those of French et al. (2016) are those of Wang et al. (2020) and Scuderi et al. (2017). The former use pressure rates of 2.0 MPa/min and 0.5 MPa/min. The latter use a smaller rate of 0.017 MPa/min. For $d_c = 0.02$ mm, $v_0 = 3.0 \times 10^{-7}$ m/s and $\sigma = 50$, the corresponding values of $\dot{P}_\infty$ are 0.044, 0.011 and 3.8×10^{-4}.

Another experiment imposing a pore pressure rate is that of Noël et al. (2019). They impose a sinusoidal pressure variation. Using the maximum pressure rate and other parameters from their experiment gives $\dot{P}_\infty$ in the range 0.015 to 0.120 for a displacement rate of 10^{-3} mm/s and an order of magnitude smaller for 10^{-4} mm/s. The range of $\dot{P}_\infty$ is where the rapid decrease of effective stress quickly stabilizes any instabilities due to RS effects. These estimates are consistent with their inference that the onset of slip corresponds to the reduction of the effective stress and that larger amplitudes induce the onset earlier.

The spring mass system is a primitive model of faulting. Nevertheless, we can make some connection with the study of Almakari et al. (2019). They simulate slip on a heterogeneous fault governed by RS friction and examine the seismicity rate increase due to a ramp increase in pore pressure at an injection site. The rates range from 0.01 to 10 MPa/day. σ = 100 MPa and $v_0 = 10^{-9}$ m/s. Their values of d_c vary along the fault and range from 0.01 to 0.37 mm. Using a value of $d_c = 0.1$ mm, in the middle of this range, a pressure rate 10 MPa/d and the values of σ and v_∞ yield $\dot{P}_\infty = 0.012$. This is about the same as for the French et al. (2016) experiment and at the upper range of where there is a competition between slip events due to RS friction and the rapid decrease of effective stress.

An important limitation of the simulations is that we have taken the normal stress as constant. In the standard axisymmetric compression tests changes of normal and shear stress are coupled by the geometry and in their experiments French et al. (2016) also alter the lateral stress which changes the normal stress on the slip surface. Rudnicki and Chen (1988) have used a slip-weakening model to examine the interaction of pore pressure effects with normal stress changes in experiments by Brace and Martin (1968) and Chambon and Rudnicki (2001) extended Segall and Rice (1995) to include normal stress changes. Neither of these studies included pore pressure rate changes. Another of changes in the normal stress neglected here is on state as identified by Linker and Dieterich (1992). This effect has been included in the simulations of Andrés et al. (2019) (although they did not look at the effect of pressure rate.

French et al. (2016) give some interpretation of their results in terms of RS effects but they do not measure values of the parameters a, b and d_c and the appropriate values are uncertain. Marone et al. (1990) found $d_c = 0.02$ mm from velocity stepping experiments on gouge layers of Ottawa sand and this value is probably reasonable for a sandstone. For a and b we have simply used representative magnitudes with $b > a$ in order to have velocity weakening and instability. Furthermore, there are indications that the values of a, b and d_c change with pore pressure and imposed slip rate (Scuderi & Collettini, 2016; Noël et al., 2019; Cappa et al., 2019).

In spite of the differences between the model and the experiment of French et al. (2016) the calculated stress drops and maximum slip rates are consistent with those observed in the experiments. For $\hat{c} = 10$ and $\dot{P}_\infty = 10^{-3}$ maximum slip rates are about two orders of magnitude greater than v_0, in rough agreement with the experiment (Figure 3d of French et al. (2016)). Similarly, stress drops from the calculations are similar to those in the experiments. Stress drops from Figure 4c of French et al. (2016) are 0.5 to 2.0 MPa. In the calculations they are slightly larger, about 3.0 to 4.0 MPa (0.04 to 0.05 $\times 50/\mu_0$ MPa). Admittedly, this agreement is based on the arbitrary choice of $\hat{k} = 0.1$. Maximum slip rates and stress drops for $\hat{k} = 0.5$ are much smaller. (See Supporting Information.)

There are, however, some clear discrepancies between the experiment and the simulations. French et al. (2016) observe a pore pressure increase, indicating compaction, accompanies slip instability. The magnitude of the increase is about 55 % of the shear stress drop and the increase is permanent. The simulations show a decrease of pressure with instability and then an increase with magnitude much smaller than observed in the experiment. One possible explanation is that the (nondimensional) pressure rate in the experiment is about 10^{-2} at which the rapid downward trend of the effective stress strongly stabilizes RS effects. Compaction and dilation in the formulation here, and in Segall and Rice (1995), are entirely associated with RS effects. (Segall and Rice (1995) remove a linear trend from the observations of Marone et al. (1990) to estimate RS parameters.)

The compaction observed by French et al. (2016) may be due to the neglect of normal stress changes in the simulations.

6 Conclusion

We have investigated the system of a spring and a mass sliding on a surface governed by RS friction. The pore pressure on the surface is coupled to the value in a remote reservoir. As Segall and Rice (1995) have shown, the model, although very simple, has a rich range of responses. The effects of increasing pore pressure in the reservoir further enrich this range. The analysis is motivated by observations that induced seismicity depends on injection rate and by experiments that examine the effect of pressure rate. The simulations illustrate the effects of pressure rate and diffusivity on the type, magnitude, frequency, and stress drop of slip events. Using parameters from the experiments of French et al. (2016) and Marone et al. (1990), we find that interaction of effects due to the pressure rate and RS friction are significant within a relatively narrow (a few orders of magnitude) range of pressure rates and diffusivity. Within this range, the frequency of slip events increases with increases in the pressure rate and maximum slip rates do not appear to be significantly affected by the pressure rate. More importantly, we find that RS instabilities are predicted to occur during the duration of an experiment only for a limited range of (non-dimensional) diffusivity and pressure rate. This range is similar to the pressure rates and diffusivities in the experiments of French et al. (2016), Noël et al. (2019), and Wang et al. (2020) and the field simulations of Almakari et al. (2019). Although the spring block configuration is simple, these simulations can aid in the interpretation of experiments and provide guidance for field studies.

Acknowledgments
No new data was used in this manuscript. Y.Z. thanks the University of Science and Technology Beijing for support and Northwestern University for hosting him during his visit from July 1, 2018 to January 1, 2019. JWR thanks Ghassan Shahin for assistance with the typesetting. We are grateful to reviewers Chris Marone and Paul Segall for their insightful comments that significantly improved the manuscript.

References

Almakari, M., Dublanchet, P., Hervé, C., & Frédéric, P. (2019). Effect of the injection scenario on the rate and magnitude content of injection-induced seismicity: Case of a heterogeneous fault. *Journal of Geophysical Research*, *124*, 8426-8448. doi: 10.1029/2019jb017898

Andrés, S., Santillán, D., Mosquera, J. C., & Cueto-Felgueroso, L. (2019). Delayed weakening and reactivation of rate-and-state faults driven by pressure changes due to fluid injection. *Journal of Geophysical Research*, *124*, 11,917-11,937. doi: 10.1029/2019.JB018109

Barbour, A. J., Norbeck, J. H., & Rubinstein, J. L. (2017). The effects of varying injection rates in Osage County, Oklahoma, on the 2016 Mw 5.8 Pawnee earthquake. *Seismological Research Letters*, *88*(4), 1040-1053.

Bhattacharya, P., Rubin, A. M., Bayart, E., Savage, H. M., & Marone, C. (2015). Critical evaluation of state evolution laws in rate and state friction: Fitting large velocity steps in simulated fault gouge with time-, slip-, and stress-dependent constitutive laws. *Journal of Geophysical Research*, *120*, 6365-6385. doi: 10.1002/2015JB012437

Brace, W. F., & Martin, R. J., III. (1968). A test of the law of effective stress for crystalline rocks of low porosity. *International Journal of Rock Mechanics and Mining Sciences*, *5*, 415-426.

Cappa, F., Scuderi, M. M., Collettini, C., Guglielmi, Y., & Avouac, J.-P. (2019).

Stabilization of fault slip by fluid injection in the laboratory and in situ. *Science Advances*, *5*(eaau4065). doi: 10.1126/sciadv.aau4065

Chambon, G., & Rudnicki, J. W. (2001). Effects of normal stress variations on frictional stability of a fluid-infiltrated fault. *Journal of Geophysical Research*, *106*(B6), 11,353-11,372.

Dieterich, J. H. (1979). Modeling of rock friction, 1, experimental results and constitutive equations. *Journal of Geophysical Research*, *84*, 2161-2168.

Ellsworth, W. L. (2013). Injection-induced earthquakes. *Science*, *341*. doi: 10.1126/science.1225942

French, M. E., Zhu, W., & Banker, J. (2016). Fault slip controlled by stress path and fluid pressurization rate. *Geophysical Research Letters*, *43*, 4330-4339. doi: 10.1002/2016GL068893

Goebel, T. H. W., Weingarten, M., X., C., Haffener, J., & Brodsky, E. E. (2017). The 2016 Mw 5.1 Fairview, Oklahoma earthquakes: Evidence for long-range poroelastic triggering at > 40 km from fluid disposal wells. *Earth and Planetary Science Letters*, *472*, 50-61. doi: 10.1016/j.epsl.2017.05.011

Green, D. H., & Wang, H. F. (1994). Shear wave velocity and attenuation from pulse-echo studies of Berea sandstone. *Journal of Geophysical Research*, *99*(B6), 11755 - 11763. doi: 10.10.1029/94JB00506

Horton, S. (2012). Disposal of hydrofracking waste fluid by injection into subsurface aquifers triggers earthquake swarm in central Arkansas with potential for damaging earthquake. *Seismological Research Letters*, *83*(2), 250-260. doi: 10.1785/gssrl.83.2.250

Keranen, K. M., Savage, H. M., Abers, G. A., & Cochran, E. S. (2013). Potentially induced earthquakes in Oklahoma, USA: Links between wastewater injection and the 2011 Mw 5.7 earthquake sequence. *Geology*, *41*(6), 699-702. doi: 10.1130G34045.1

Keranen, K. M., Weingarten, M., Abers, G. A., Bekins, B. A., & Ge, S. (2014). Sharp increase in central Oklahoma seismicity since 2008 induced by massive wastewater injection. *Science*, *345*(6195), 448-451. doi: 10.1126/science.1255802

Linker, M. F., & Dieterich, J. H. (1992). Effects of variable normal stress on rock friction: observations and constitutive equations. *Journal of Geophysical Research*, *97*, 4923-4940.

Marone, C. (1998). Laboratory - derived friction laws and their application to seismic faulting. *Annual Reviews of Earth and Planetary Science*, 643-696.

Marone, C., Raleigh, C. B., & Scholz, C. H. (1990). Frictional behavior and constitutive modeling modeling of simulated fault gouge. *Journal of Geophysical Research*, *95*, 7007 - 7025.

Noël, C., Passelégue, F. X., Giorgetti, C., & Violay, M. (2019). Fault reactivation during fluid pressure oscillations: Transition from stable to unstable slip. *Journal of Geophysical Research*, *124*, 10,940-10,953. doi: 10.1029/2019JB018517

Passelégue, F. X., Brantut, N., & Mitchell, T. M. (2018). Fault reactivation by fluid injection: controls from stress state and injection rate. *Geophysical Research Letters*, *45*, 12,837-12846. doi: 10.1029/2018GL080470

Rice, J. R. (1993). Spatio-temporal complexity of slip on a fault. *Journal of Geophysical Research*, *98*(B6), 9885-9907.

Rice, J. R., & Tse, S. T. (1986). Dynamic motion of a single degree of freedom system following a rate and state dependent friction law. *Journal of Geophysical Research*, *91*(B1), 521-530.

Rudnicki, J. W., & Chen, C.-H. (1988). Stabilization of rapid frictional slip on a weakening fault by dilatant hardening. *Journal of Geophysical Research*, *93*, 4745-4757.

Ruina, A. (1983). Slip instability and state variable friction laws. *Journal of Geophysical Research*, *88*, 10,359-10,370.

Scuderi, M. M., & Collettini, C. (2016). The role of fluid pressure in induced vs. triggered seismicity: insights from rock deformation experiments on carbonates. *Nature Scientific Reports*. doi: 10.1038/srep24852

Scuderi, M. M., Collettini, C., & Marone, C. (2017). Frictional stability and earthquake triggering during fluid pressure stimulation of an experimental fault. *Earth and Planetary Science Letters*, *477*, 84-96.

Segall, P., & Rice, J. R. (1995). Dilatancy, compaction, and slip instability of a fluid-infiltrated fault. *Journal of Geophysical Research*, *100*(B11), 22155-22171.

Wang, L., Kwiatek, G., Rybacki, E., Bonnelye, A., Bohnhoff, M., & Dresen, G. (2020). Laboratory study on fluid-induced fault slip behavior: The role of fluid pressurization rate. *Geophysical Research Letters*, *47*(e2019GL086627). doi: 10.1029/2019GL086627

Weingarten, M., Ge, S., Godt, J. W., Bekins, B. A., & Rubinstein, J. L. (2015). High-rate injection is associated with the increase in U.S. mid-continent seismicity. *Science*, *348*(6241), 1336-1340.

Wibberley, C. A. J., & Shimamoto, T. (2003). Internal structure and permeability of major fault zones: The Median Tectonic Line in Mie Prefecture, Southwest Japan. *Journal of Structural Geology*, *25*, 49-78.

Zhang, S., & Tullis, T. (1998). The effect of fault slip on permeability and permeability anisotropy in quartz gouge. *Tectonophysics*, *298*(1-2), 41-52.

Zoback, M. D., & Byerlee, J. D. (1976). Effect of high-pressure on permeability of Ottawa sand. *American Association of Petroleum Geologists Bulletin*, *60*, 1531-1542.